Electromagnetic Modes in Conical Transmission Lines with Application to the Linearly Tapered Slot Antenna

Benoît Stockbroeckx and André Vander Vorst, *Fellow, IEEE*

***Abstract*—A transmission line analysis of bow-tie antenna and linearly tapered slot antenna (LTSA) is presented. These structures belong to the class of conical transmission lines defined here in terms of conical coordinates. A complete set of solutions of Helmholtz equation is obtained exhibiting TE and TM modes. Modal fields are expressed by Lamé and Bessel–Schelkunoff functions. TE and TM eigenmode analysis is particularized to the bow-tie structure. Bow-tie antenna and LTSA are shown to be dual conical transmission lines by the image method and Babinet's principle. The modes of LTSA are calculated on the basis of the results obtained for the bow-tie structure. The radiation pattern of LTSA is computed as the integral of a closed-form expression of the dyadic Green's function weighted by the modal electric field distribution over the slot aperture. The obtained dominant mode radiation patterns are validated by measurements from the literature. The radiation patterns of the first two-order modes are calculated and compared.**

***Index Terms*—Conical transmission lines, slot antennas.**

I. Introduction

THE linearly tapered slot antenna (LTSA) is depicted in Fig. 1. It consists of one sector of flare angle φ_0 cut in a metallic half-plane. The antenna is fed by a classical slot transmission line at the sector apex. LTSA has been first proposed in 1979 [1] for applications in short-range radar module and as an element for phased-array antenna at 9 GHz. Several applications of LTSA have been proposed at increasing frequencies like the broken line tapered-slot antenna (BLTSA), which is derived from the original LTSA. BLTSA has been used in 1993 in a radiometer operating at 802 GHz [2]. We have used [3]–[5] the present LTSA analysis for modeling the Vivaldi antenna [4]. In the present paper, it is shown that LTSA and bow-tie (Fig. 2) shapes are dual, using Babinet's principle and the image method. So that the LTSA, BLTSA, and Vivaldi analyses are obtained from the bow-tie analysis.

The electric current distribution on the bow tie is calculated in [6] from results of [7] by applying two conformal mappings. It yields the TEM dominant mode of the structure. This mode is used in [8] for the LTSA radiation calculation. The computation of such analytical results requires only a small central processing unit (CPU) time. On the other hand, a full numerical analysis of the LTSA and Vivaldi antenna is proposed in [9] where the electromagnetic fields are computed by using the TLM method. Full numerical analyses and simulations with commercially available electromagnetic softwares are CPU time consuming due to the large extent of the tapered antennas and do not yield any modal description of the fields in the structure.

The present analysis of the bow-tie structure is based on the conical coordinate system [10], also called sphero-conal coordinate system [11]. This system depicts three sets of coordinate

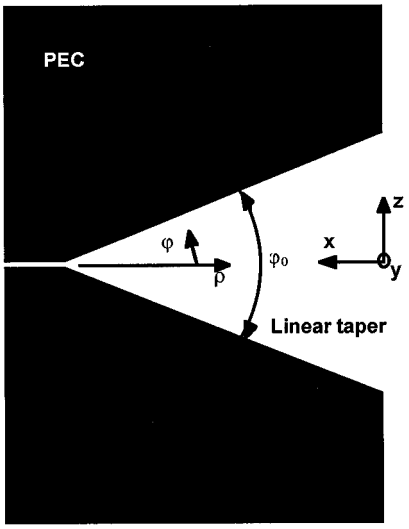

Fig. 1. Linearly tapered-slot antenna (LTSA) with flare angle φ_0 fed by classical slot transmission line.

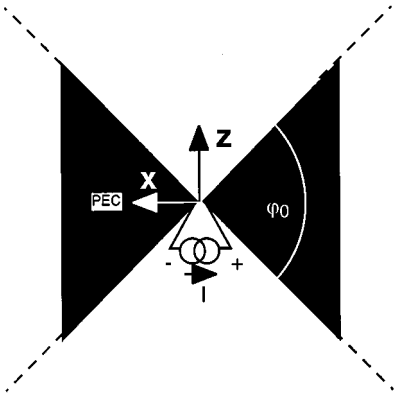

Fig. 2. Bow-tie antenna with flare angle φ_0 fed by balanced electric current source.

Manuscript received November 30, 1998; revised December 2, 1999. This work was supported in part by the Government of the Walloon Region, Belgium, under the FIRST program.

The authors are with Laboratoire d'Hyperfréquences, Université catholique de Louvain, Louvain-la-Neuve, B-1348 Belgium.

Publisher Item Identifier S 0018-926X(00)02457-1.

surfaces: two sets of bicones having an elliptical section and one set of concentric spheres. Such a coordinate system is consistent with the conical waveguide boundary conditions (metallic elliptical cone) [12] so that Helmholtz equation can be solved by separating the variables. The two metallic sectors of the bow-tie structure (Fig. 2) are obtained by degenerating the metallic elliptical bicone of the conical waveguide into a flat conical waveguide having an elliptical cross-section of infinite eccentricity. The so-obtained bow-tie structure is also called flat biconical antenna. It is characterized by its flare angle noted φ_0 (Fig. 2). This method, using the conical transmission line theory, yields all the eigenmodes of the bow-tie structure, not only the TEM dominant mode.

The first part of the paper presents a complete set of solutions for Helmholtz equation in the conical coordinate system. They are obtained by separating the variables, and correspond to TE and TM modes. They are particularized to the bow-tie structure in the second part. The third part is dedicated to the LTSA analysis. The duality between bow-tie and LTSA structures is shown. The electric field distribution across the slot is calculated, as well as the radiation pattern of the TEM and TE_1 modes. The sensitivity of the radiation pattern to power losses in the conductor is finally analyzed.

II. Conical Transmission Line Theory

A. Conical Coordinate System [10]

Conical coordinates (r, θ, λ) describe an orthogonal system (Fig. 3) [10] related to the classical rectangular system by

$$\begin{cases} x^2 = \left(\dfrac{r\theta\lambda}{bc}\right)^2 \\ y^2 = \dfrac{r^2(\theta^2-b^2)(b^2-\lambda^2)}{b^2(c^2-b^2)} \\ z^2 = \dfrac{r^2(c^2-\theta^2)(c^2-\lambda^2)}{c^2(c^2-b^2)} \end{cases} \tag{1}$$

with $0 < \lambda^2 < b^2 < \theta^2 < c^2$. The surfaces generated by imposing $r = \text{constant}$ are concentric spheres centered on $(0,0,0)$. The surfaces generated by $\theta = \text{constant}$ are confocal cones with elliptical section, vertex at $(0,0,0)$, focal plane (x,z), and focal angle $\varphi_0 = 2\arcsin(b/c)$ around Oz axis. The surfaces generated by $\lambda = \text{constant}$ are confocal cones with elliptical section, vertex at $(0,0,0)$, focal plane (x,z), and focal angle $180 - \varphi_0 = 2\arccos(b/c)$ around Ox axis.

By inspection of (1) it is observed that x, y, and z are functions of r, θ, and λ with parameters b and c. They can be rewritten so that x, y, and z are functions of r, θ/c, and λ/c with parameter b/c, respectively, in which c appears as a normalization constant and can be set equal to one. Parameter b is now related more clearly to the focal angle by writing $b = \sin(\varphi_0/2)$.

B. Solutions of Helmholtz Equation

Following Harrington [13], electromagnetic fields and Helmholtz equation can be written in terms of the magnetic $(\bar{\mathbf{A}})$ and electric $(\bar{\mathbf{F}})$ vector potentials, and the electric (Φ^a) and magnetic (Φ^f) scalar potentials. As demonstrated in [13],

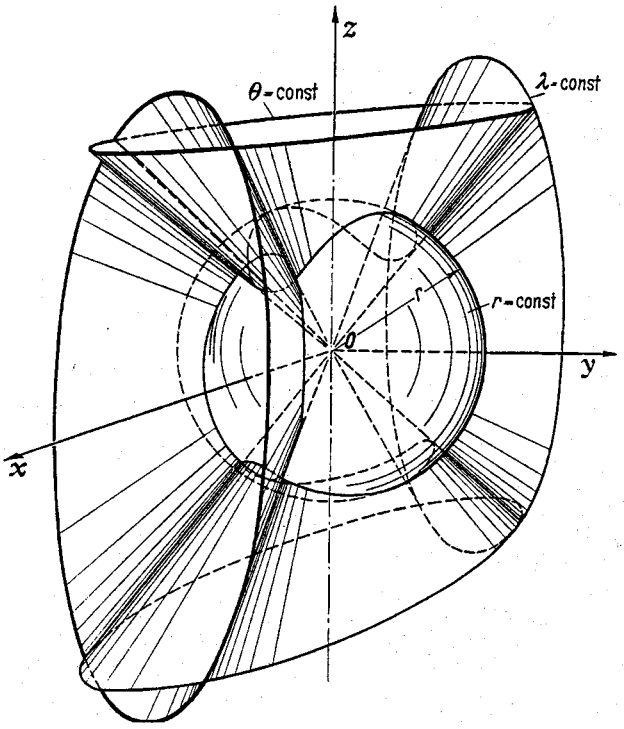

Fig. 3. Conical coordinate system (r, θ, λ) related to rectangular coordinate system (x, y, z) [10].

a complete set of independent solutions of Helmholtz equation is obtained by defining two classes of solutions. The first class is obtained by imposing (2), while the second class is obtained by imposing (3)

$$\begin{cases} \bar{\mathbf{A}} = \bar{\mathbf{0}} \\ \bar{\mathbf{F}} = f\bar{\mathbf{a}}_{\mathbf{r}} \end{cases} \tag{2}$$

$$\begin{cases} \bar{\mathbf{A}} = a\bar{\mathbf{a}}_{\mathbf{r}} \\ \bar{\mathbf{F}} = \bar{\mathbf{0}} \end{cases} \tag{3}$$

Solving Helmholtz equation, one obtains

$$\begin{cases} -j\omega\varepsilon\Phi^a = \dfrac{\partial a}{\partial r} \\ -j\omega\mu\Phi^f = \dfrac{\partial f}{\partial r} \end{cases}$$

which yields two second-order partial differential equations

$$\nabla \times \nabla \times (a\bar{\mathbf{a}}_{\mathbf{r}})|_r - k^2 a = \frac{\partial^2 a}{\partial r^2} \tag{4}$$

$$\nabla \times \nabla \times (f\bar{\mathbf{a}}_{\mathbf{r}})|_r - k^2 f = \frac{\partial^2 f}{\partial r^2} \tag{5}$$

Modes are obtained by calculating the solutions of the first class, using (2). The corresponding fields have no radial component of electric field $(E_r = 0)$. These modes are consequently called TE. Other modes are obtained by calculating the solutions of the second class using (3). The corresponding fields have no

radial component of magnetic field ($H_r = 0$). These modes are consequently called TM.

The curl operators in (4) and (5) are developed by using the expression of the differential operators in conical coordinates [10]. Because (4) and (5) have the same form, only one set of general solution is developed by separation of variables

$$a, f = R(r)\Theta(\theta)\Lambda(\lambda) \tag{6}$$

which yields three second-order ordinary differential equations

$$\frac{d^2R}{dr^2} + \left[k^2 - \frac{n(n+1)}{r^2}\right] R = 0 \tag{7}$$

$$\begin{aligned}(\theta^2 - b^2)(\theta^2 - 1)\frac{d^2\Theta}{d\theta^2} + \theta[2\theta^2 - (b^2+1)]\frac{d\Theta}{d\theta} \\ + [q(b^2+1) - n(n+1)\theta^2]\Theta = 0\end{aligned} \tag{8}$$

$$\begin{aligned}(\lambda^2 - b^2)(\lambda^2 - 1)\frac{d^2\Lambda}{d\lambda^2} + \lambda[2\lambda^2 - (b^2+1)]\frac{d\Lambda}{d\lambda} \\ + [q(b^2+1) - n(n+1)\lambda^2]\Lambda = 0\end{aligned} \tag{9}$$

where n and q are separation constants.

Equation (7) is the Bessel–Schelkunoff equation [13] with as solutions the Bessel–Schelkunoff functions $\hat{B}_n(kr) = krb_n(kr) = \sqrt{\pi kr/2}B_{n+1/2}(kr)$, where $B_{n+1/2}(kr)$ is a cylindrical Bessel function of semi-integer order $n + 1/2$ and $b_n(kr)$ is a spherical Bessel function of integer order n. The Bessel functions are of the first, second, or third kind. Bessel functions of the first and second kinds (J and Y) are well suited for describing standing waves in a radially bounded structure, while Hankel functions (or Bessel functions of the third kind $H^{(1,2)}$) are well suited for describing forward and reverse traveling waves in a radially semi-infinite structure. As we are interested with propagating modes in a semi-infinite transmission line, the Hankel functions are used

$$R = \sqrt{\frac{\pi kr}{2}}\left[AH^{(1)}_{n+\frac{1}{2}}(kr) + BH^{(2)}_{n+\frac{1}{2}}(kr)\right] \tag{10}$$

which degenerate to circular harmonics for $n = 0$.

Equations (8) and (9) are Lamé equations. Solutions are expressed in terms of Lamé polynomials of the first and second kinds, of order n and parameter q (see Appendix for more details):

$$\Theta = CE^C_n(q_n, \theta) + DF^C_n(q_n, \theta) \tag{11}$$

$$\Lambda = GE^C_n(q_n, \lambda) + IF^C_n(q_n, \lambda) \tag{12}$$

where C is the class of the function, depending on the order n.

III. Bow-Tie Analysis

The bow-tie structure is depicted in Fig. 2. The two metallic sectors lay in the (x, z) plane with a sector angle around Ox axis. Following Section II-A, this part of the structure corresponds to the particular coordinate surfaces $\lambda = \pm b = \pm\sin(\varphi_0/2)$ of Fig. 3. On the other hand, the two slot sectors lay in the (x, z) plane with a sector angle around Oz axis. Following Section II-A, this part of the structure corresponds to the particular coordinate $\theta = \pm b$ of Fig. 3.

A. TE Modes

The electric field components of TE modes are given by (2), (6), and (10)–(12). The boundary conditions are imposed by the two metallic sectors on which the tangential component of the electric field vanishes and by the two slot sectors on which the normal component of the electric field vanishes due to symmetry. The solution for order $n = 0$ is then

$$\begin{cases} E_r = 0 \\ E_\theta = 0 \\ E_\lambda = \dfrac{1}{\sqrt{\theta^2 - \lambda^2}}\dfrac{1}{r}(Ae^{jkr} + Be^{-jkr}) \end{cases} \tag{13}$$

$$\begin{cases} H_r = 0 \\ H_\theta = j\sqrt{\dfrac{\varepsilon}{\mu}}\dfrac{1}{\sqrt{\theta^2 - \lambda^2}}\dfrac{1}{r}(Ae^{jkr} - Be^{-jkr}) \\ H_\lambda = 0 \end{cases} \tag{14}$$

This zeroth-order mode is a TE mode which is degenerated into a TEM one. The solution for order $n = 1$ and parameter $q = 1$ is

$$\begin{cases} E_r = 0 \\ E_\theta = \sqrt{\dfrac{\pi k}{2}}\theta\sqrt{\dfrac{(b^2 - \lambda^2)(1 - \lambda^2)}{\theta^2 - \lambda^2}} \\ \qquad \times \left[\displaystyle\int_0^b \frac{d\theta}{\theta^2\sqrt{\theta^2 - b^2}\sqrt{\theta^2 - 1}} \right. \\ \qquad \left. - \displaystyle\int_0^\theta \frac{d\theta}{\theta^2\sqrt{\theta^2 - b^2}\sqrt{\theta^2 - 1}}\right] \\ \qquad \times \dfrac{1}{\sqrt{r}}\left[AH^{(1)}_{\frac{3}{2}}(kr) + BH^{(2)}_{\frac{3}{2}}(kr)\right] \\ E_\lambda = -\sqrt{\dfrac{\pi k}{2}}\lambda\left\{\sqrt{\dfrac{(\theta^2 - b^2)(\theta^2 - 1)}{\theta^2 - \lambda^2}}\right. \\ \qquad \times \left[\displaystyle\int_0^b \frac{d\theta}{\theta^2\sqrt{\theta^2 - b^2}\sqrt{\theta^2 - 1}} \right. \\ \qquad \left. \left. - \displaystyle\int_0^\theta \frac{d\theta}{\theta^2\sqrt{\theta^2 - b^2}\sqrt{\theta^2 - 1}}\right] - \dfrac{1}{\theta\sqrt{\theta^2 - \lambda^2}}\right\} \\ \qquad \times \dfrac{1}{\sqrt{r}}\left[AH^{(1)}_{\frac{3}{2}}(kr) + BH^{(2)}_{\frac{3}{2}}(kr)\right]. \end{cases}$$

The solution for order $n=1$ and parameter $q=q_1$ (A.9) cannot satisfy boundary conditions. The solution for order $n=1$ and parameter $q=q_2$ (A.10) is

$$\begin{cases} E_r = 0 \\ E_\theta = j\sqrt{\dfrac{\pi k}{2}}\lambda\sqrt{\dfrac{(b^2-\lambda^2)(\theta^2-1)}{\theta^2-\lambda^2}}\left[\Pi\left(b^2;\dfrac{\pi}{2}\,\middle|\,b^2\right)\right. \\ \qquad \left. -\,\Pi\left(b^2;\arcsin\left(\dfrac{\theta}{b}\right)\,\middle|\,b^2\right)\right] \\ \qquad \times\dfrac{1}{\sqrt{r}}\left[AH^{(1)}_{\frac{3}{2}}(kr)+BH^{(2)}_{\frac{3}{2}}(kr)\right] \\ E_\lambda = -\sqrt{\dfrac{\pi k}{2}}\sqrt{\lambda^2-1}\left\{j\theta\sqrt{\dfrac{\theta^2-b^2}{\theta^2-\lambda^2}}\left[\Pi\left(b^2;\dfrac{\pi}{2}\,\middle|\,b^2\right)\right.\right. \\ \qquad \left. -\,\Pi\left(b^2;\arcsin\left(\dfrac{\theta}{b}\right)\,\middle|\,b^2\right)\right] \\ \qquad \left. +\,j\sqrt{\dfrac{\lambda^2-1}{(\theta^2-\lambda^2)(\theta^2-1)}}\right\} \\ \qquad \times\dfrac{1}{\sqrt{r}}\left[AH^{(1)}_{\frac{3}{2}}(kr)+BH^{(2)}_{\frac{3}{2}}(kr)\right] \end{cases}$$

where Π is the elliptic integral of the third kind [14].

B. TM Modes

The magnetic field components of TM modes are given by (3), (6), and (10)–(12). The boundary conditions are the same as for the TE modes. The solution for order $n=0$ (zeroth-order mode) is a TM mode which is degenerated into a TEM one so that the TE_0 and the TM_0 modes both refer to the same TEM mode. This particular TEM mode is the same as the one obtained in [8] by applying two conformal mappings.

The solution for order $n=1$ and parameter $q=1$ is

$$\begin{cases} H_r = 0 \\ H_0 = -\sqrt{\dfrac{\pi k}{2}}\theta\sqrt{\dfrac{(b^2-\lambda^2)(1-\lambda^2)}{\theta^2-\lambda^2}} \\ \qquad \times\left[\displaystyle\int_0^b \frac{d\lambda}{\lambda^2\sqrt{\lambda^2-b^2}\sqrt{\lambda^2-1}}\right. \\ \qquad \left. -\displaystyle\int_0^\lambda \frac{d\lambda}{\lambda^2\sqrt{\lambda^2-b^2}\sqrt{\lambda^2-1}} - \frac{1}{\lambda\sqrt{\lambda^2-b^2}\sqrt{\lambda^2-1}}\right] \\ \qquad \times\dfrac{1}{\sqrt{r}}\left[AH^{(1)}_{\frac{3}{2}}(kr)+BH^{(2)}_{\frac{3}{2}}(kr)\right] \\ H_\lambda = \sqrt{\dfrac{\pi k}{2}}\lambda\sqrt{\dfrac{(\theta^2-b^2)(1-\theta^2)}{\theta^2-\lambda^2}} \\ \qquad \times\left[\displaystyle\int_0^b \frac{d\lambda}{\lambda^2\sqrt{\lambda^2-b^2}\sqrt{\lambda^2-1}}\right. \\ \qquad \left. -\displaystyle\int_0^\theta \frac{d\lambda}{\lambda^2\sqrt{\lambda^2-b^2}\sqrt{\lambda^2-1}}\right] \\ \qquad \times\dfrac{1}{\sqrt{r}}\left[AH^{(1)}_{\frac{3}{2}}(kr)+BH^{(2)}_{\frac{3}{2}}(kr)\right]. \end{cases}$$

IV. LTSA Analysis and Radiation Calculation

A. LTSA Definition

The electric current distribution on the right-hand sector of the bow-tie antenna remains unchanged if a perfect electric conductor is placed between the two sectors and if the balanced feeder is replaced by an unbalanced one [Fig. 4(a)]. Using Babinet's principle, such a structure is equivalent to the infinite linearly tapered slot line fed by an unbalanced magnetic current, as depicted in Fig. 4(b). The unbalanced magnetic current feeder can be realized by a slot transmission line, which yields the linearly tapered slot antenna (Fig. 1). Bow-tie antenna and LTSA are consequently dual by image method and Babinet's principle.

B. Field Distribution Calculation

Following Babinet's principle the electric field distribution across the slot of the LTSA is proportional to the magnetic field on the metallic sector of the bow-tie antenna (14) (Fig. 4). Across the slot of the LTSA ($\lambda=b$), the tangential electric field can be expressed by linking the conical coordinate system (1) and the polar coordinate system of Fig. 1, using $\varphi=\arcsin(x/r)=\arcsin(\theta)$:
for $n=0$

$$E_\varphi = \frac{1}{\sin\left(\frac{\varphi_0}{2}\right)}\frac{1}{\sqrt{1-\frac{\sin^2(\varphi)}{\sin^2\left(\frac{\varphi_0}{2}\right)}}}\frac{1}{\rho}\left(Ae^{jk\rho}+Be^{-jk\rho}\right) \quad (15)$$

for $n=1$ and parameter $q=1$

$$E_\varphi = \frac{\sin(\varphi)}{\sin^2\left(\frac{\varphi_0}{2}\right)}\frac{1}{\sqrt{1-\frac{\sin^2(\varphi)}{\sin^2\left(\frac{\varphi_0}{2}\right)}}} \times\sqrt{\frac{\pi k}{2\rho}}\left[AH^{(1)}_{\frac{3}{2}}(k\rho)+BH^{(2)}_{\frac{3}{2}}(k\rho)\right] \quad (16)$$

for $n=1$ and parameter $q=q_2=(b^2/b^2+1)$

$$E_\varphi = \frac{\cos(\varphi)}{\sin\left(\frac{\varphi_0}{2}\right)\cos\left(\frac{\varphi_0}{2}\right)}\frac{1}{\sqrt{1-\frac{\sin^2(\varphi)}{\sin^2\left(\frac{\varphi_0}{2}\right)}}} \times\sqrt{\frac{\pi k}{2\rho}}\left[AH^{(1)}_{\frac{3}{2}}(k\rho)+BH^{(2)}_{\frac{3}{2}}(k\rho)\right]. \quad (17)$$

The denominators of (15) to (17) vanish for $\varphi=\pm\varphi_0/2$ so that the electric field goes to infinity for such a polar angle. This characterizes mathematically the edge effect, which is expected at the metallic edges. Modes given by (15) and (17) are even while (16) is odd.

Equation (15) of the azimuthal field is equivalent to the transverse and longitudinal expressions given by [8, eq. (1), (2)]. The higher order modes however were not obtained in [8], while our method is general enough to give all the modes propagating on the structure.

For a long structure (typically more than two wavelengths) the incident power at the end of the transmission line is strongly reduced because of radiation ($1/\rho$ term in (15)–(17)), and the reverse traveling wave can be neglected ($A=0$).

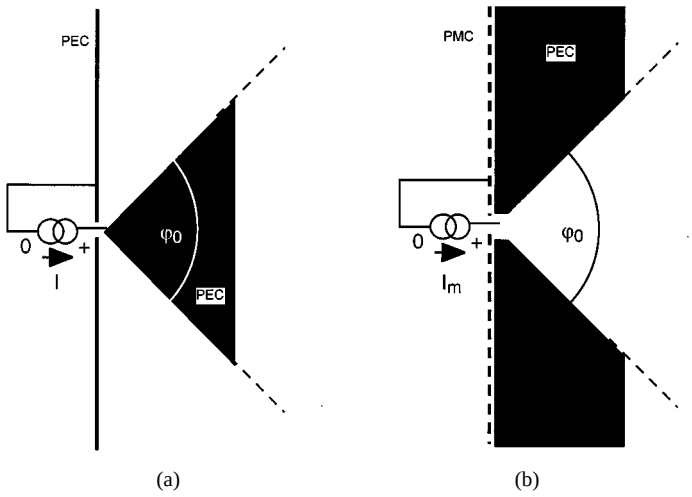

(a) (b)

Fig. 4. (a) Antenna equivalent to bow-tie (Fig. 2). (b) Antenna equivalent to LTSA [Fig. 4(a)].

Electric field distributions in (15)–(17) are valid for LTSA without dielectric substrate while most favorite in practice is LTSA etched on a dielectric slab. The effect of the dielectric layer can be taken into account by using the present results together with those of a variational method developed for multilayered structures [15]. The combination of these results is presented in [3] and [5].

C. Radiation Calculation

The radiated fields are calculated from the azimuthal electric field distribution across the slot (15)–(17). This vector field can be decomposed into two components as $E_\varphi \bar{\mathbf{a}}_\varphi = \cos(\varphi) E_\varphi \bar{\mathbf{a}}_z + \sin(\varphi) E_\varphi \bar{\mathbf{a}}_x$, where $\bar{\mathbf{a}}_z$ is the unit vector parallel to the edge and $\bar{\mathbf{a}}_x$ the unit vector perpendicular to the edge (Fig. 1). Using Green's formalism, the radiated field is given as

$$\bar{\mathbf{E}}^{(R)} = \int\int_S E_\varphi \bar{\bar{\mathbf{G}}} \cdot [\cos(\varphi)\bar{\mathbf{a}}_z + \sin(\varphi)\bar{\mathbf{a}}_x]\, dS \tag{18}$$

where S is the tapered slot aperture and $\bar{\bar{\mathbf{G}}}$ is the dyadic Green's function. Green's function and radiated field are expressed in the spherical coordinate system (r, θ^e, φ^e) linked to the rectangular system (x, y, z) of Fig. 1. Superscript e indicates that the system is bound to the edge of the structure. In reference to the dominant mode field distribution, the half-plane $\varphi^e = 180°$ is called the E-plane and the plane $\theta^e = 90°$ is called the H-plane. In reference to the dominant mode radiation (Section IV-C.2), the θ^e-component of the radiated electric field is the copolar field and the φ^e-component is the cross-polar field.

The analytical expression of the Green's function is calculated in [16] for the copolar field in the E and H-planes. We calculate it for both copolar and cross-polar fields for any direction [3], [5]. Green's dyadic is given as

$$\bar{\bar{\mathbf{G}}} = \begin{pmatrix} G^{\theta,z} & 0 \\ G^{\varphi,z} & G^{\varphi,x} \end{pmatrix} \tag{19}$$

where $G^{\theta,z}$ yields the copolar radiated field due to a longitudinal electric field source (parallel to $\bar{\mathbf{a}}_x$), while $G^{\varphi,z}$ and $G^{\varphi,x}$ yield the cross-polar radiated field due to a longitudinal and a radial (parallel to $\bar{\mathbf{a}}_z$) electric field source, respectively. The closed-form expressions are

$$\begin{aligned}
G^{\theta,z} &= -\frac{e^{j\frac{\pi}{4}}}{\sqrt{2\pi}} \frac{e^{-jkr}}{r} k e^{jkz\cos\theta^e} \\
&\quad \times \left\{ j|\sin\varphi^e| e^{jkx\sin(\theta^e)\cos(\varphi^e)} F[kx\sin(\theta^e) \right. \\
&\quad \left. \times (1+\cos\varphi^e)] + \sin\left(\frac{\varphi^e}{2}\right) \frac{e^{-jkx\sin\theta^e}}{\sqrt{\pi kx\sin\theta^e}} \right\} \\
G^{\varphi,z} &= -\frac{e^{j\frac{\pi}{4}}}{\sqrt{2\pi}} \frac{e^{-jkr}}{r} k\cos(\theta^e) e^{jkz\cos\theta^e} \\
&\quad \times \left\{ \pm j\cos(\varphi^e) e^{jkx\sin(\theta^e)\cos(\varphi^e)} F[kx\sin(\theta^e) \right. \\
&\quad \left. \times (1+\cos\varphi^e)] + \cos\left(\frac{\varphi^e}{2}\right) \frac{e^{-jkx\sin\theta^e}}{\sqrt{\pi kx\sin\theta^e}} \right\} \\
G^{\varphi,x} &= \mp j \frac{e^{j\frac{\pi}{4}}}{\sqrt{2\pi}} \frac{e^{-jkr}}{r} k\sin(\theta^e) e^{jkz\cos\theta^e} e^{jkx\sin(\theta^e)\cos(\varphi^e)} \\
&\quad \times F[kx\sin(\theta^e)(1+\cos\varphi^e)]
\end{aligned} \tag{20}$$

where F is Fresnel's integral defined as

$$F(x) = \int_0^x \frac{e^{-jt}}{\sqrt{2\pi t}}\, dt$$

Some comments on these expressions can be found in [5]. In particular, the practical case where the conductor half-sheet is longitudinally finite is discussed in this reference.

The double integral (18) can be reduced to a single one [8] in case of a small flare angle and dominant mode excitation. Otherwise the double integral has to be performed, normally numerically.

1) Validation by Measured Results: The simulated TEM mode radiation pattern of the LTSA is validated by measurements previously published in [8]. The antenna is $5\lambda_0$ long and the flare angle is 15°. Simulations and measurements are compared in Fig. 5 for (a) the H-plane and (b) the E-plane. The agreement is good. The accuracy obtained with our model is the same as the one obtained in [8]. Nevertheless our model yields the copolar and cross-polar radiated fields for all the modes (Figs. 6 and 7), which cannot be computed with the model proposed in [8]. The cross-polar radiation levels cannot be validated because such measured results are not available for LTSA without substrate. Nevertheless the crosspolar field validation is presented for Vivaldi antennas on dielectric substrate in [5].

2) Dominant Mode and Higher Order Mode Radiation: The dominant TEM mode radiation patterns are obtained by using (15) and (18)–(20), while the TE_1 mode radiation patterns are obtained by using (16) and (18)–(20). The radiation properties of the two modes are compared in terms of polarization and isotropy. Fig. 6 depicts the copolar radiated fields of the TEM and TE_1 modes in the E-plane. The main lobe of the *TEM copolar* radiation is centered in the endfire direction $(\theta^e = 90°)$, while the main lobe of the $\mathbf{TE_1}$ *copolar* radiation is oriented in another direction, which is about $\theta^e = 70°$. In the E-plane, there is no cross-polar radiation for both modes. Fig. 7 depicts the H-plane radiation patterns of both modes (*copolar* for *TEM*

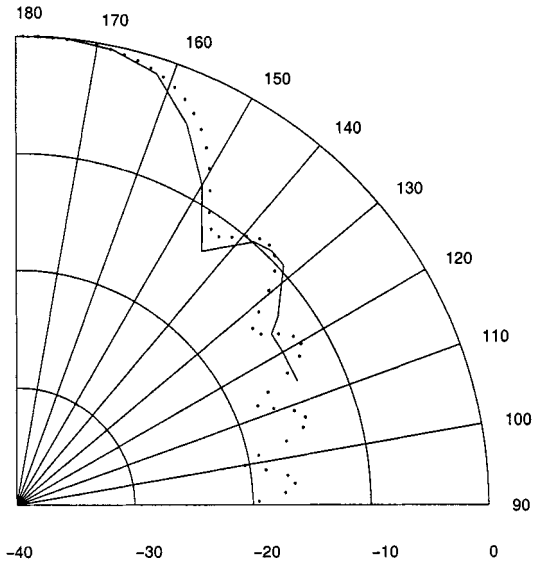

(a)

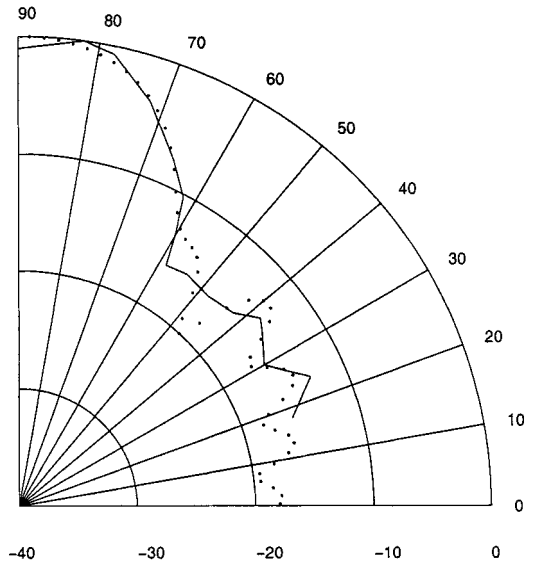

(b)

Fig. 5. Measured [8] $(-)$ and calculated $(\cdot)$ (a) H- and (b) E-plane radiation patterns, LTSA without substrate $5\lambda_0$ long and 15° flare angle.

and *crosspolar* for $\mathbf{TE_1}$). The TEM mode radiates in the endfire direction $(\varphi^e = 180°)$, while the TE_1 mode exhibits a more isotropic radiation pattern than the TEM mode. Consequently, there is a particular high backfire $(\varphi^e = 0°)$ level for the TE_1 mode. In the H-plane, there is no cross-polar radiation for the TEM mode and no copolar radiation for the TE_1 mode. The TE_1 mode radiated field is consequently crosspolarized with respect to the TEM mode radiated field in that plane.

D. Power Losses in Conductor

Taking into account the finite conductivity of the metal yields two consequences. The first is an exponential field amplitude attenuation along the taper. This attenuation is taken into account in the term E_φ of the integrand in (18), which affects the result of the integral. In the case of a good conductor the power losses are low. Then the attenuation along the taper is low when compared to the $1/\rho$ attenuation in (15)–(17) and is neglected. The second consequence is a nonvanishing tangential component of the electric field on the conductor surface. This causes a radial electric field component on the conductor, which is perpendicular to the azimuthal component across the slot. Such a radial field causes cross polarization. The tangential electric field component on the metal can be calculated by a perturbation method. Assuming that the magnetic field calculated without losses (14) remains unchanged when low losses are introduced, and assuming that the metal thickness is much larger than the skin depth, the tangential electric field is related to the tangential magnetic field (14) by the metal impedance. The ratio between the tangential electric field amplitude on the metal and the electric field amplitude across the slot is then given as the product of the metal impedance and the free-space admittance. For copper at 24 GHz this ratio is $0.15\ 10^{-3}$. The radial field is consequently negligible when compared to the azimuthal field.

As a consequence, the radiation pattern of LTSA is not sensitive to the power losses in the conductor.

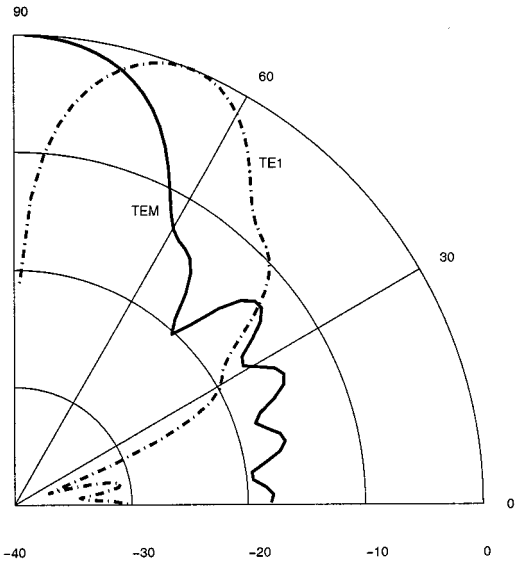

Fig. 6. Copolar E-plane radiation pattern of TEM $(-)$ and TE_1 $(-\cdot)$ modes, LTSA without substrate.

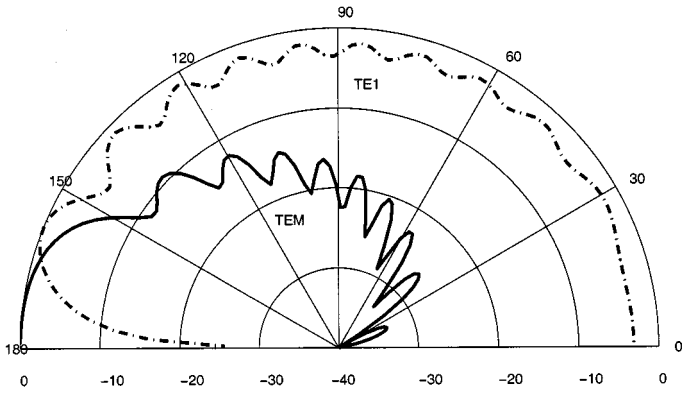

Fig. 7. H-plane radiation pattern of TEM $(-)$ mode, copolar, and $TE_1(-\cdot)$ mode, cross-polar LTSA without substrate.

V. Conclusion

The electromagnetic fields of the eigen modes propagating in conical structures made of lossless conductors in a homogeneous lossy dielectric medium have been calculated analytically. TE and TM modes yield a complete set of solutions of Helmholtz equations.

The bow-tie antenna is shown to be a conical transmission line with a degenerated elliptical section and the conical eigen mode theory is particularized to that structure. The bow-tie antenna and the LTSA are dual structures, as shown by application of Babinet's principle and the image method. The electric field distribution in the slot aperture of LTSA is obtained for the first three-order modes by using duality. This yields the edge effect at the metallic edges, the curvature of the field across the tapered slot, and all the modes propagating in the structure. Moreover, the accuracy of the method is sufficient for radiation calculation. The calculated copolar radiation patterns of a TEM LTSA have been compared to measurements published in the literature. The accuracy of the simulation is good. The first two-order mode radiation patterns have been compared. In the E-plane, the main lobe of the TEM mode is oriented in the endfire direction, while that of the TE_1 mode is oriented in the direction $\theta = 70°$. In the H-plane, the TE_1 mode radiation is cross polarized relatively to the TEM mode radiation. The H-plane radiation pattern of the TE_1 mode is more isotropic than the TEM mode and exhibits a high backfire level. The power losses due to the conductor finite conductivity are shown to have a negligible effect on radiation.

Those results are obtained without using time consuming computational methods. No numerical difficulties have been observed during computation, which is remarkable.

Appendix
Lamé Equation and Functions

Lamé equation is obtained when expressing Laplace equation in ellipsoidal and conical coordinates and Helmholtz equation in conical coordinates. It is given as

$$(t^2-b^2)(t^2-c^2)\frac{d^2T}{dt^2}+t[2t^2-(b^2+c^2)]\frac{dT}{dt} + [q(b^2+c^2)-n(n+1)t^2]T=0. \tag{A.1}$$

The functions, solutions of (A1), have been introduced by Gabriel Lamé in 1837 [17] while solving Laplace equation in ellipsoidal coordinates for calculating heat distribution in a homogeneous ellipsoid. They are classically based on series of increasing powers of t^2

$$f(t^2)=\sum_{i=0}^{+\infty} d_i t^{2i}. \tag{A.2}$$

Four classes are distinguished [18]

$$\text{I} \quad T=f(t^2) \tag{A.3}$$

$$\text{II} \quad \begin{cases} T=tf(t^2) \\ T=\sqrt{t^2-b^2}f(t^2) \\ T=\sqrt{t^2-c^2}f(t^2) \end{cases} \tag{A.4}$$

$$\text{III} \quad \begin{cases} T=t\sqrt{t^2-b^2}f(t^2) \\ T=t\sqrt{t^2-c^2}f(t^2) \\ T=\sqrt{t^2-b^2}\sqrt{t^2-c^2}f(t^2) \end{cases} \tag{A.5}$$

$$\text{IV} \quad T=t\sqrt{t^2-b^2}\sqrt{t^2-c^2}f(t^2). \tag{A.6}$$

Coefficients d_i (A.2) of the power series in (A.3)–(A.6) are calculated by inserting (A3)–(A.6) in (A.1) and identifying coefficients of t of equal power. Lamé polynomials are a set of Lamé functions based on particular values of q such that the series (A.2) reduces to a polynomial in t^2. The value of q is obtained by imposing the vanishing of $d_{n/2+1}$ for class I, $d_{(n-1)/2+1}$ for class II, $d_{(n-2)/2+1}$ for class III, and $d_{(n-3)/2+1}$ for class IV. This imposition is called the characteristic equation. It has a number of solutions depending on order n and on the class considered. Each solution q of the characteristic equation yields a new Lamé polynomial so that there is a number of solutions of (A.1) depending on the class considered. The question of notation is troublesome since there are almost as many notations as investigators. We adopt here a notation such that Lamé polynomials are denoted by $E_n^C(q,t)$ where n is the order and C the class of the polynomial (1 for class I, 21 to 23 for class II, 31 to 33 for class III or 4 for class IV), parameter q being the solution of the characteristic equation. The first Lamé polynomials corresponding to values of n (the order) from zero to two are listed below. The series is normalized by putting $d_0 = 1$

$$\mathbf{n=0} \quad q=0 \quad E_0^1(0,t)=1 \tag{A.7}$$

$$\mathbf{n=1} \quad q=1 \quad E_1^{21}(1,t)=t \tag{A.8}$$

$$q=\frac{c^2}{b^2+c^2}=q_1 \quad E_1^{22}(q_1,t)=\sqrt{t^2-b^2} \tag{A.9}$$

$$q=\frac{b^2}{b^2+c^2}=q_2 \quad E_1^{23}(q_2,t)=\sqrt{t^2-c^2} \tag{A.10}$$

$$\mathbf{n=2} \quad q=2+2\frac{\sqrt{b^4+c^4-b^2c^2}}{b^2+c^2}=q_3$$
$$E_2^1(q_3,t)=1-\frac{b^2+c^2+\sqrt{b^4+c^4-b^2c^2}}{b^2c^2}t^2 \tag{A.11}$$

$$q=2-2\frac{\sqrt{b^4+c^4-b^2c^2}}{b^2+c^2}=q_4$$
$$E_2^1(q_4,t)=1-\frac{b^2+c^2-\sqrt{b^4+c^4-b^2c^2}}{b^2c^2}t^2 \tag{A.12}$$

$$q=\frac{b^2+4c^2}{b^2+c^2}=q_5 \quad E_2^{31}(q_5,t)=t\sqrt{t^2-b^2} \tag{A.13}$$

$$q=\frac{4b^2+c^2}{b^2+c^2}=q_6 \quad E_2^{32}(q_6,t)=t\sqrt{t^2-c^2} \tag{A.14}$$

$$q=1 \quad E_2^{33}(1,t)=\sqrt{t^2-b^2}\sqrt{t^2-c^2}. \tag{A.15}$$

General theory of second-order differential equations shows that if one solution of the equation is known, then a second solution independent of the first one can be obtained by integration [19]. This is particularized here as

$$F_n^C(q,t)=AE_n^C(q,t)\int\frac{dt}{\sqrt{(t^2-b^2)(t^2-c^2)}\left[E_n^C(q,t)\right]^2}$$

where A is an arbitrary constant. Lamé functions of the second kind $F_n^C(q,t)$, linearly independent of $E_n^C(q,t)$, have been calculated and are listed below for $n=0$ and 1

$$\mathbf{n=0} \quad q=0 \quad F_0^1(0,t)=E\left[\arcsin\left(\frac{t}{b}\right)\,\middle|\,\frac{b^2}{c^2}\right]$$

where $E[\cdot]$ is the elliptic integral of the first kind with amplitude $\arcsin(t/b)$ and modulus b/c [14]

$$\mathbf{n=1} \quad q=1 \quad F_1^{21}(1,t)=t\int\frac{dt}{t^2\sqrt{(t^2-b^2)(t^2-c^2)}}$$

$$q=\frac{c^2}{b^2+c^2}=q_1$$
$$F_1^{22}(q_1,t)=\sqrt{t^2-b^2}\Pi\left[1;\arcsin\left(\frac{t}{b}\right)\,\middle|\,\frac{b^2}{c^2}\right]$$

where $\Pi[\cdot]$ is the elliptic integral of the third kind with parameter 1, amplitude $\arcsin(t/b)$ and modulus b/c [14]

$$q=\frac{b^2}{b^2+c^2}=q_2$$
$$F_1^{23}(q_2,t)=\sqrt{t^2-c^2}\Pi\left[\frac{b^2}{c^2};\arcsin\left(\frac{t}{b}\right)\,\middle|\,\frac{b^2}{c^2}\right].$$

It can be shown [20] that Lamé polynomials $E_n^C(q,t)$ of same class, same order, and different q are linearly independent. The general solution of (A.1) is then expressed as

$$T(t)=\sum_{n=0}^{+\infty}\left[A_nE_n^C(q_n,t)+B_nF_n^C(q_n,t)\right].$$

REFERENCES

[1] S. N. Prasad and S. Mahapatra, "A novel MIC slot-line antenna," in *Proc. 9th Eur. Microwave Conf.*, Brighton, U.K., Sept. 1979, pp. 120–124.

[2] P. R. Acharya, H. Ekström, S. S. Gearhart, S. Jacobsson, J. F. Johansson, E. L. Kollberg, and G. M. Rebeiz, "Tapered slotline antennas at 802 GHz," *IEEE Trans. Microwave Theory Tech.*, vol. 41, pp. 1715–1719, Oct. 1993.

[3] B. Stockbroeckx, "Space Wave and Surface Wave Radiation in the Vivaldi Antenna," Ph.D. dissertation, Catholic Univ. Louvain, Louvain-la-Neuve, Belgium, 1998.

[4] P. J. Gibson, "The vivaldi aerial," in *Proc. 9th Eur. Microwave Conf.*, Brighton, U.K., Sept. 1979, pp. 101–105.

[5] B. Stockbroeckx and A. Vander Vorst, "Copolar and crosspolar radiation of vivaldi antenna on dielectric substrate," *IEEE Trans. Antennas Propagat.*, vol. 48, pp. 19–25, Jan. 2000.

[6] R. C. Compton, R. C. McPhedran, Z. Popovic, G. M. Rebeiz, P. P. Tong, and D. B. Rutledge, "Bow-tie antennas on dielectric half-space: Theory and experiment," *IEEE Trans. Antennas Propagat.*, vol. AP-35, pp. 622–631, June 1987.

[7] R. L. Carrel, "The characteristic impedance of two infinite cones of arbitrary cross section," *IRE Trans. Antennas Propagat.*, vol. AP-6, no. 2, pp. 197–201, Apr. 1958.

[8] R. Janaswamy, D. H. Schaubert, and D. M. Pozar, "Analysis of the transverse electromagnetic mode linearly tapered slot antenna," *Radio Sci.*, vol. 21, no. 5, pp. 797–804, Sept./Oct. 1986.

[9] F. Ndagijimana, "Développement et application de la méthode TLM à l'étude des antennes dérivées de la ligne à fente," Ph.D. dissertation, INPG, Grenoble, France, 1990.

[10] P. Moon and D. E. Spencer, *Field Theory Handbook*. Berlin, Germany: Springer-Verlag, 1961.

[11] S. Blume and V. Krebs, "Numerical evaluation of dyadic diffraction coefficients and bistatic radar cross sections for a perfectly conducting semi-infinite elliptical cone," *IEEE Trans. Antennas Propagat.*, vol. 46, pp. 414–424, Mar. 1998.

[12] J. K. M. Jansen, "Simple Periodic and Nonperiodic Lamé Functions and Their Application in the Theory of Conical Waveguides," Ph.D. dissertation, Eindhoven Univ. Technol., Eindhoven, The Netherlands, 1976.

[13] R. F. Harrington, *Time-Harmonic Electromagnetic Fields*. New York: McGraw-Hill, 1961.

[14] M. Abramowitz and I. A. Stegun, *Handbook of Mathematical Functions*. New York: Dover, 1965.

[15] I. Huynen, D. Vanhoenacker, and A. Vander Vorst, "Spectral domain form of new variational expression for very fast calculation of multilayered lossy planar line parameters," *IEEE Trans. Microwave Theory Tech.*, vol. 42, no. 11, pp. 2099–2106, Nov. 1994.

[16] R. Janaswamy and D. H. Schaubert, "Analysis of the tapered slot antenna," *IEEE Trans. Antennas Propagat.*, vol. AP-35, pp. 1058–1064, Sept. 1987.

[17] G. Lamé, "Mémoire sur les surfaces isothermes dans les corps solides homogènes en équilibre de température," *J. Mathématiques Pures et Appliquées (J. Liouville)*, vol. 2, pp. 147–183, 1837. 1ère série, Tome 2.

[18] P. Humbert, *Mémorial des sciences mathématiques: Fonctions de Lamé et fonctions de Mathieu*. Paris, France: Académie des sciences de Paris, 1926.

[19] P. M. Morse and H. Feshbach, *Methods of Theoretical Physics*. New York: McGraw-Hill, 1953.

[20] F. M. Arscott, *Periodic Differential Equations*, London, U.K.: Pergamon, 1964.

Benoît Stockbroeckx was born in Brussels, Belgium, in 1970. He received the Electrical Engineer and Ph.D. (applied sciences) degrees from the Université catholique de Louvain (UCL), Louvain-la-Neuve, Belgium, in 1993 and 1998, respectively.

In 1993, he joined the Microwave Laboratory at UCL. From 1993 to 1994 he investigated YIG resonators. Since 1994 he has been working on wide-band slotline antenna and Vivaldi antenna modeling. His research interest is in microwave planar circuit modeling.

André Vander Vorst (M'64–SM'68–F'86) was born in Brussels, Belgium, in 1935. He received the Electrical and Mechanical Engineer and Ph.D. (applied sciences) degrees from the Université catholique de Louvain (UCL), Belgium, in 1958 and 1965, respectively, and the M.Sc. degree in electrical engineering from the Massachusetts Institute of Technology (MIT), Cambridge, in 1965.

He is with UCL, Belgium, where he became Assistant in 1958, Assistant Professor in 1962, Associate Professor in 1968, and Professor in 1972. From 1958 to 1964 he worked on fast switching of magnetic cores. With a NATO fellowship, he was in the United States from 1964 to 1966, first at MIT, then at Stanford University, CA, both in the field of radio astronomy. In 1966, he founded the Microwave Laboratory at UCL, Belgium, which he is still heading. He has been involved in all the research activities of the Laboratory, starting with loaded waveguides and cavities, then with atmospheric transmission and diffraction up to 300 GHz, designing and measuring active and passive circuits up to and above 100 GHz, and microwave bioelectromagnetics. He was Head of the Electrical Engineering Department 1970–1972, Dean of Engineering 1972–1975, Vice-President of the Academic Council 1973–1975, President of the Open School in Economic and Social Politics 1973–1987, all at UCL, Belgium. He has authored or coauthored three textbooks, several chapters, and a variety of scientific and technical papers in international journals and proceedings. His present interests are with microwave-optical transducers, humanitarian demining, and the interaction of electromagnetic fields with the nervous system.

Dr. Vander Vorst is a member of the National Committee of URSI and of various committees on communications, microwaves, and education. He has been active in IEEE Region 8 as well as in the European Microwave Conferences. He is a member of Academia Europaea and The Electromagnetics Academy. He received the Sitel Prize 1986 and the Meritorious Service Award of the MTT Society, IEEE in 1994.